ChemPubSoc Europe

DOI: 10.1002/cctc.201701940

CHEMCATCHEM Full Papers

Oxidative Dehydrogenation of *n*-Octane over Niobium-Doped $NiAl_2O_4$: An Example of Beneficial Coking in Catalysis over Spinel

Majid D. Farahani, Venkata D. B. C. Dasireddy, and Holger B. Friedrich*[a]

$NiAl_2O_4$-based materials are known as enhanced catalysts for several catalytic applications that have coke deposition in common. In this study, Nb as a dopant was found to occupy the octahedral sites of the spinel preferably. As a result, the cation distribution was altered between the two sub-lattices of the cubic spinel. Therefore, ordered modifications of nickel migration, electronic profile, redox properties and surface textures were observed for these catalysts. Also, coke deposition over these catalysts was controlled using Nb doping and found to modify the original features of the fresh catalysts and lower their crystallite sizes. This study suggests reasons why $NiAl_2O_4$ spinel performs so well in the majority of the high-temperature catalytic processes that suffer from coke deposition.

Introduction

Nickel aluminate is a member of the spinel family with the general formula of AB_2O_4 and is known to have a magneto-plumbite-like structure.[1–3] Preparation techniques for the synthesis of $NiAl_2O_4$ include coprecipitation,[3,4] sol–gel,[5] solid-state reaction,[6] the alkoxide method,[7,8] Pechini,[9,10] and combustion synthesis.[11,12] $NiAl_2O_4$ had been used for the partial oxidation of methane, methane (steam or dry) reforming,[9] oxidative coupling of methane,[13] diesel steam reforming,[14,15] tar reforming,[16] and tetradecane reforming.[17] $NiAl_2O_4$ is known to have an inverse spinel structure, and the degree of this inversion can be varied by modifying the preparation technique and the temperature of the synthesis.[6,9,18–21] Furthermore, migration of nickel between the two sub-lattices (changing the degree of inversion) or to the $NiAl_2O_4$ surface is well established and seems to be highly dependent on catalytic reaction conditions.[9]

Substituting the dopant atoms (even in small quantities) in the lattice of a host oxide can have profound influences on the properties of the host, such as morphology changes, changes in electronic and transport properties and lower transition temperatures. These are important parameters in heterogeneous catalysis.[22] Material-based studies on doped $NiAl_2O_4$ have shown some significant changes, such as ion migration upon the occupancy of foreign metals and modifications in the lattice constant.[20,23]

Coke formation in oxidative dehydrogenation (ODH) (especially under anaerobic conditions) is expected. The coke can cover the surface and deactivate the catalyst during paraffin activation.[24]

However, exceptions are known to the above-mentioned phenomena, and some examples of beneficial coking exist, in which catalytic reactions were enhanced upon coke formation.[25–27] The reported reasons for profitable coking are that deposited coke acts as active sites, the selective deactivation of nonselective catalytic sites and the participation of the formed coke in the catalytic reactions.[28] Interestingly, $NiAl_2O_4$ is found to be active in catalytic reactions that normally suffer from coke formation and minimises coke deposition.[13,15] However, there is no detailed explanation for this behaviour, and more investigations seem to be required. Furthermore, $NiAl_2O_4$ is highly stable in catalytic applications that involve coking.

Beside, few reports exist that discuss the effect of foreign-metal doping in the lattice of these binary metal oxides and their physicochemical characteristics.[20,21,23] Therefore, this study focuses on the modification of the physical and chemical properties of this structure upon coke deposition. Nb was chosen as a dopant because of its interesting chemistry such as acting as high-valance dopant (HVD) or low-valance dopant (LVD) in the form of $Nb_2O_4^{2-}$ and the modification of electroconductivity of nickel-based materials by diminishing the number of positive holes, if doped into the NiO lattice and used for the oxidative dehydrogenation of ethane.[29–32] Also, it has a similar atomic radius to those of Ni and Al, making it a suitable substituent. Several physicochemical characterisation techniques were used to identify the changes caused by Nb doping in this system. Then, these catalysts were used for the ODH of *n*-octane under "anaerobic conditions". Afterwards, the used materials were fully characterised to see how the coking influenced the composition of these catalysts. Finally, the crucial role of coking in catalysis over $NiAl_2O_4$ is discussed. *n*-Octane was chosen as a model substrate, because medium-

[a] Dr. M. D. Farahani, Dr. V. D. B. C. Dasireddy, Prof. H. B. Friedrich
School of Chemistry and Physics
University of KwaZulu-Natal
Durban 4000 (South Africa)
E-mail: friedric@ukzn.ac.za

Supporting information and the ORCID identification number(s) for the author(s) of this article can be found under: https://doi.org/10.1002/cctc.201701940.

chain length paraffins are abundant and of low intrinsic value.[33,34]

Results

X-ray diffraction (XRD) and inductively coupled plasma optical emission spectroscopy (ICP–OES)

It has been shown that sol–gel auto combustion using oxalyldihdrazide facilitates the synthesis of $NiAl_2O_4$.[12] However, a high calcination temperature (≈1000 °C) is required for the synthesis of pure-phase $NiAl_2O_4$.[9] The targeted elemental compositions were achieved and confirmed by using inductively coupled plasma optical emission spectroscopy ICP–OES (Table 1). The powder XRD (PXRD) data of the prepared catalysts are shown in Figure 1a. The absence of any nickel oxide phase was confirmed by XRD analysis for all four catalysts. The

Table 1. Elemental and phase compositions of the as prepared catalysts.

Catalyst	Ni[a]	Nb[a]	L[b] [nm]	
			fresh	used
SP	1.00	–	22.9	12.00
SP-0.02 Nb	0.98	0.02	29.4	12.6
SP-0.06 Nb	0.97	0.06	25.1	15.6
SP-0.10 Nb	0.95	0.10	31.8	21.5

[a] The atomic ratio between the elements according to ICP–OES. [b] Average crystallite size of $NiAl_2O_4$ estimated using the Scherrer equation.

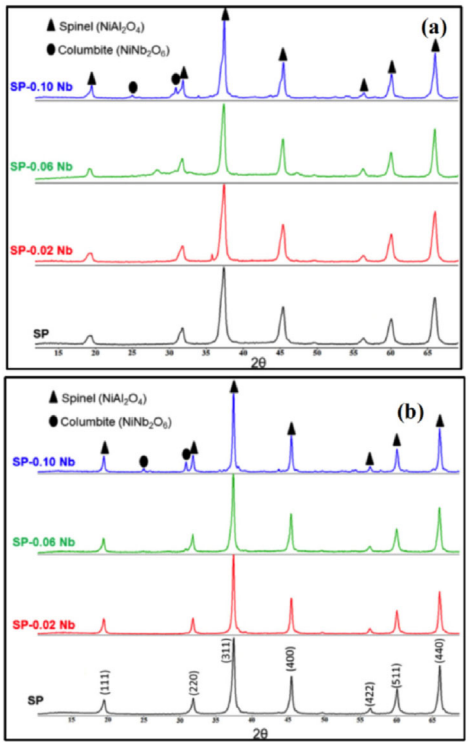

Figure 1. PXRD patterns of a) as-prepared catalysts, b) used catalysts.

XRD patterns of $NiAl_2O_4$ (SP) and $NiAl_2O_4$ containing 0.02 at.% Nb (SP-0.02 Nb) showed only the peaks of spinel (ICDD PDF#78-0552) (Figure 1a). The formation of the $NiNb_2O_6$ phase (ICDD PDF#00-032-0694) was detected when higher concentrations of Nb precursors were used for the syntheses of SP-0.06 Nb and SP-0.10 Nb (Figure 1a). This phase belongs to the columbite family and is known to be inert under oxidative dehydrogenation reaction conditions.[35,36] Also, there are a few small peaks at $2\theta \approx 38°$, 43°, and 54°, which belong to the columbite phase.[35] In addition, the high intensity of the peaks in the XRD diffractograms suggest a high degree of crystallinity for these catalysts, which is driven by the high-temperature treatment during the synthesis. The calculated average crystallite sizes of the spinels, using the Scherrer equation, for all catalysts showed an increase in crystallite size with the introduction of niobium (Table 1), except SP-0.06 Nb. The small loading of Nb in SP-0.02 Nb caused a noticeable increase of crystallite size if compared to SP. However, further increase of Nb doping (in SP-0.06 Nb) and slight formation of $NiNb_2O_6$ seems to minimise the crystal growth effect that was observed for SP-0.02 Nb, and result in a slight increase of crystallite size of $NiAl_2O_4$ spinel if compared to SP. Also, the catalyst with the highest Nb doping (SP-0.10 Nb) showed the largest crystallite size. The observed pattern is probably the result of induced synergic effects owing to $NiNb_2O_6$ formation and the amount of Nb doping in different quantities for each catalyst.

No change in the XRD peak positions for the fresh and used catalysts is observed, which is proof of the thermal stability of these materials under the reaction conditions (after 48 h at 500 °C). The intensity of all the spinel peaks had decreased after the reactions and small shoulders appeared on the left side of each peak that belong to different spinel facets (Figure S9). This implies smaller crystallite sizes for the used catalysts compared to what was observed for the fresh catalysts and slight structural alteration during the catalytic application. The crystallite sizes for the used catalysts are tabulated in Table 1. Generally, the crystallite sizes increased with Nb content for these used materials. Further studies on the XRD patterns of these catalysts were performed to probe the possibility of Nb substitution into the spinel cubic lattice.

According to reports, the planes (220) and (422) are sensitive to cation distribution in the tetrahedral (T_d) sub lattice of the cubic spinel.[20,23,37] Normally, an increase in intensities of the peaks corresponding to these planes suggests substitution in the T_d sites. Otherwise, the octahedral (O_h) site is the host for the foreign element.[20,23,37] As shown in Figure 2, the intensities of both peaks decreased if 0.02 atomic% nickel was substituted with niobium in SP-0.02 Nb, indicating the replacement of nickel in the O_h sub-lattice in this molecule. However, a different behaviour was observed if the molecular formula was chosen to result in Nb replacing both Al and Ni ions. The data, in Figure 2, shows that substitution can take place in both sub-lattices based on the available ionic vacancies in the spinel structure. Also, the formation of $NiNb_2O_5$ shows that the substitution of Nb in the spinel lattice is partial. The same trend of substitution in the sub-lattices was observed for the used catalysts, suggesting the retention of the original struc-

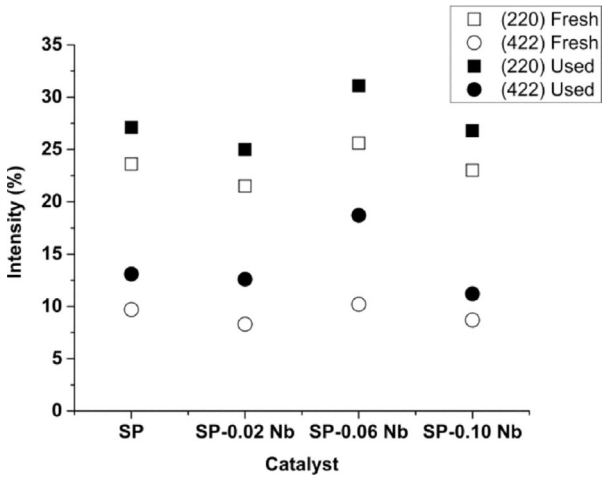

Figure 2. Change in intensities of plane (220) and (422) in the fresh and used catalysts. (The intensity of the peak with an *hkl* value of (311) was used as a reference in each diffractogram).

tures. However, some nickel ions seem to have migrated from the O_h to the T_d sites or left the lattice of spinel, as the intensities of both planes were consistently higher than what was observed for the fresh catalysts. This change shows that levels of inversion for the under study spinels decrease during the catalytic reactions.

Ultraviolet diffuse reflectance spectroscopy (UV–DRS) analysis

To investigate the coordination of Ni^{2+} in these catalysts further, ultraviolet diffuse reflectance spectroscopy (UV–DRS) spectra were obtained. The bands at 716 nm and 640 nm result from d–d electron transition of the Ni^{2+} in the O_h and T_d sub lattices of spinel, respectively.[13,38] The low concentration of introduced Nb in SP-0.02 Nb seems to replace the Ni^{2+} in O_h positions and motivate the migration of Ni^{2+} in O_h sites to the T_d sites, as the intensities of the peaks at 716 and 640 in the UV spectrum of SP-0.02 Nb are, respectively, lower and higher than those of SP (Figure 3). However, niobium in SP-0.06 Nb

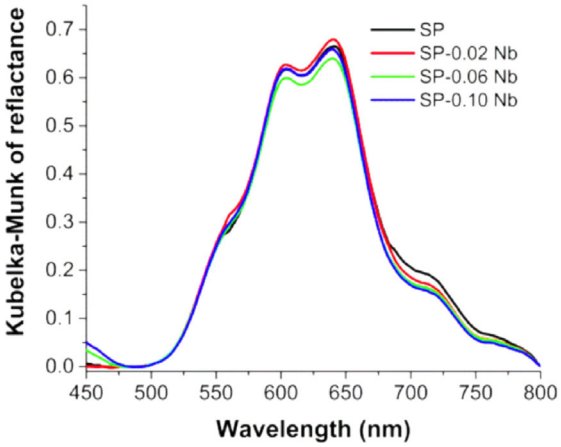

Figure 3. UV-DRS data of the SP-*x* Nb catalysts (*x*: 0, 0.02, 0.06 and 0.10).

seems to replace both Al^{3+} and Ni^{+2} ions in the O_h and T_d sub-lattices and results in weaker peaks for both sites, than for the other catalysts (Figure 3). The highest concentration of Nb doping (and the lowest molar ratio of Ni^{2+}), in SP-0.10 Nb, showed the lowest Ni^{+2} concentration in O_h sites, whereas T_d coordinated Ni^{2+} occupancy was similar to that of the undoped spinel (Figure 3). Thus, the UV–DRS and XRD data suggest Nb prefers to be octahedrally coordinated and motivates the Ni^{2+} migration if any ionic vacancies are present in the tetrahedral sub-lattice (based on the molar ratio between Ni and Al).

Nitrogen physisorption analysis

The BET surface areas and pore volumes of the catalysts decreased with the addition of niobium (Table 2). However, no regular trend was observed in the change of pore diameter for

Table 2. Surface area, pore volume and pore diameter of SP-*x* Nb catalysts (*x*: 0.0–0.1).

Catalyst	BET surface area [$m^2 g^{-1}$]		Pore volume [$cm^3 g^{-1}$]		Pore diameter [nm]	
	fresh	used	fresh	used	fresh	used
SP	17	22	0.04	0.10	10.4	17.7
SP-0.02 Nb	13	15	0.03	0.08	8.2	19.9
SP-0.06 Nb	11	12	0.02	0.05	8.5	17.9
SP-0.10 Nb	8	8	0.01	0.01	8.3	6.6

the different catalysts. Also, the N_2 adsorption–desorption isotherms showed that the observed porosity for these catalysts originated from the voids between the particles, as the hysteresis loops were at a high relative pressure (Figure S10). The nitrogen physisorption measurements of the used catalysts showed higher surface areas, pore volumes and pore diameters than the fresh catalysts. The difference between the physical properties of the fresh and used catalysts is significant for SP-0.02 Nb, and the difference becomes smaller as the concentration of the niobium phase increases in the catalyst mixtures.

TEM and SEM analysis

These catalysts showed hexagonal morphology as shown in Figure 4a. Both $NiAl_2O_4$ and $NiNb_2O_6$ have this morphology, and hence they cannot be separately identified.[35] To investigate the distribution of all three elements in these catalysts, energy dispersive X-ray spectrometry (EDX) mapping analysis was performed in DFSTEM (dark-field scanning transmission electron microscopy) mode using high-resolution transmission electron microscopy (HRTEM). Formation of $NiAl_2O_4$ always results in a good dispersion of nickel. Also, no clusters containing Nb were detected in SP-0.06 Nb Figure 4b, even if some $NiNb_2O_6$ was detected as the additional phase in the PXRD pattern (Figure 1). The HRTEM images show that both the $NiAl_2O_4$ and $NiNb_2O_6$ phases positively contributed to the observed high dispersion for these catalysts. SEM images showed

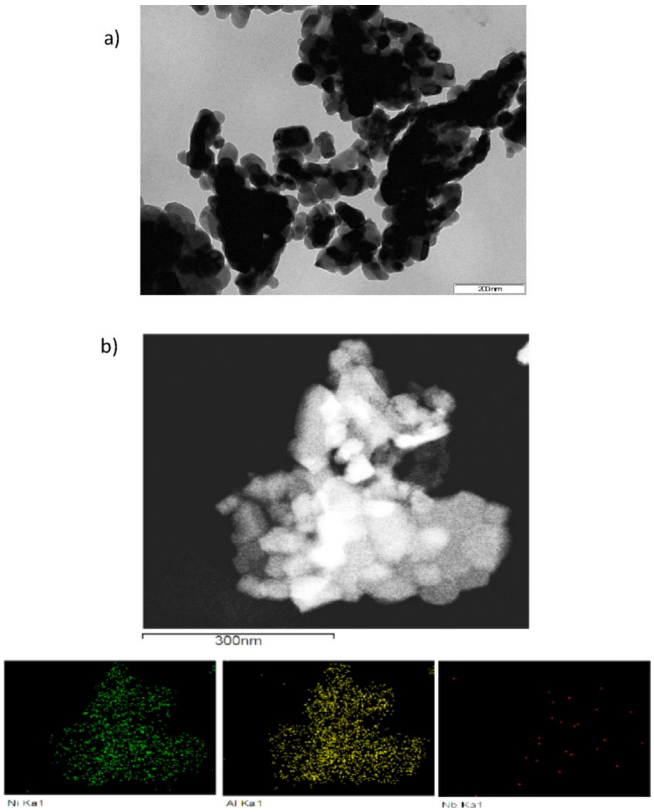

Figure 4. a) General TEM image of the as-prepared catalysts. b) Mapping analysis of Sp-0.06 Nb using HRTEM (DFSTEM mode).

sponge-shaped morphology, and the introduction of niobium seems to decrease the size of these spongy particles (Figure 5).

X-ray photoelectron spectroscopy (XPS) analysis

The XP spectra of the spinel-based catalysts are shown in Figure 6. The Ni 2p scan normally shows two main peaks, Ni $2p_{1/2}$ and Ni $2p_{3/2}$, with their related satellite peaks.[9] A separation of 6.3 ± 3.0 eV was found between the main peaks and their representative satellite, and this is known to be indicative of nickel bound in $NiAl_2O_4$, whereas pure NiO has a separation of 7.1 ± 1.0 eV and was not observed in this study.[3] The main peaks of Ni $2p_{3/2}$ were deconvoluted to further investigate the available nickel species in these catalysts. The red graphs in the Ni $2p_{3/2}$ spectra (Figure 6) with the binding energy of 853.9–855.8 eV in all catalysts shows the available Ni^{2+} in the octahedral sites of the spinel structure (Table 3).[39] The pink graph in the Ni $2p_{3/2}$ spectra (Figure 6) with the binding energy of 856.4–857.1 eV is representative of strongly bonded Ni^{3+} on the surface of the $NiAl_2O_4$ spinel (Table 3).[39,40] The green graph in the Ni$2p_{3/2}$ spectrum of SP (Figure 6) with the binding energy of 858.9 eV shows the NiO/Al_2O_3 (Table 3) and is only seen for SP as also detected in H_2 temperature-programmed reduction analysis (H_2-TPR). SP and SP-0.10 Nb have similar structures, except for the observation of the NiO/Al_2O_3 XPS peak in SP, which was not detected by XRD analysis, possibly because of the detection limit of that technique. SP-0.02 Nb has mainly octahedrally coordinated Ni^{2+} and a very small quantity of Ni^{3+} on the surface of catalyst. SP-0.06 Nb showed only Ni^{2+} with octahedral coordination.

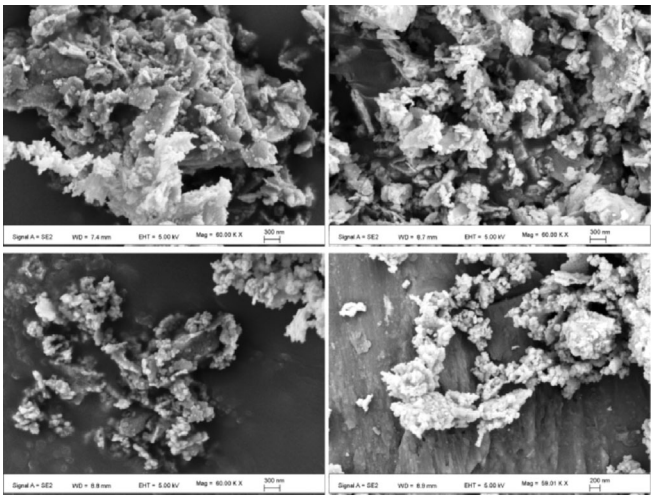

Figure 5. SEM images of SP-*x* Nb catalysts [*x*: a) 0.00, b) 0.02, c) 0.06 and d) 0.10].

The XP spectrum of O 1s is shown in Figure 6. The binding energy of 529.2 eV is typical of the metal–oxygen bond.[39] The observed peak at approximately 531.5 eV represents oxygen ions in low coordination at the surface.[39] SP and SP-0.10 Nb showed very similar types of oxygen on the surface and ionic oxygen seems to be dominant for SP-0.02 Nb. However, only oxygen atoms from the M–O bond are seen for SP-0.06 Nb. The ionic oxygen refers to the available lattice oxygens (O^{2-}) that are exposed on the surface in ionic form and normally are present in the vicinity of defect sites.[39,41] The observed order

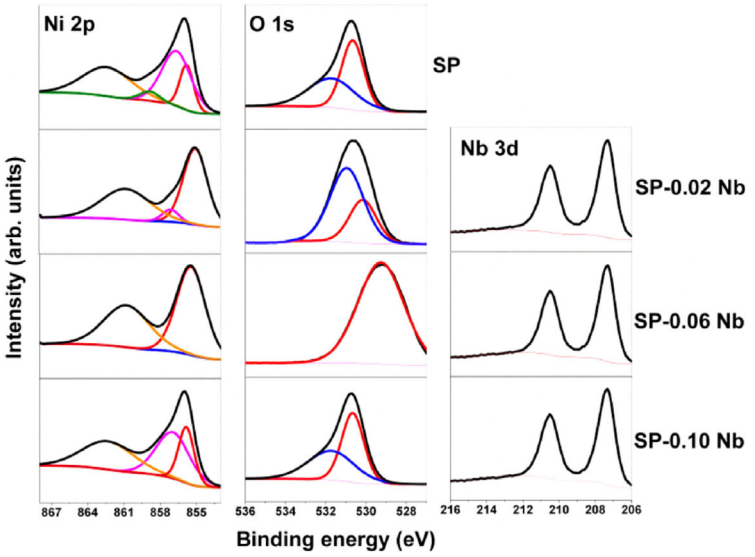

Figure 6. XP spectra of SP-*x* Nb. [*x*: a) 0.00, b) 0.02, c) 0.06 and d) 0.10] Deconvolutions of the core-level spectra Ni 2p, O 1s are provided.

Table 3. Surface compositions of the fresh catalysts determined by XPS.

Catalyst	Ni $2p_{3/2}$			O 1s		Nb 3d	Theo.	Exp.
	NiO	$Ni^{3+}/NiAl_2O_4$	Ni^{2+} [Oct]	$O_{(ion)}$	M–O	(doublet)	(Nb/Ni)	(Nb/Ni)
SP	858.9	856.7	855.8	531.7	530.7	–	0/1	0/1.17
SP-0.02 Nb	–	856.4	854.3	529.9	528.9	210.5, 207.3	0.02/0.98	0.03/1.14
SP-0.06 Nb	–	–	853.9	–	529.2	210.5, 207.4	0.06/0.97	0.07/1.20
SP-0.10 Nb	–	857.1	855.2	531.7	530.7	210.5, 207.3	0.10/0.95	0.12/1.14

for O^{2-} on the defect sites is SP-0.02 Nb > SP ≈ SP-0.10 Nb > SP-0.06 Nb. Therefore, this data shows that a higher concentration of Ni^{3+} on the surface does not necessarily create more defect sites, and that there is a limitation to which doping can generate more defect sites. The Nb 3d scan showed a doublet at 210.5 and 207.3 eV for all samples, which indicates the presence of Nb^{5+} in all catalysts.[42,43] No change in the binding energies of the observed doublet for Nb 3d in all catalysts implies an indirect role of this element in the changing of the physicochemical properties of these catalysts.

The surface compositions of these catalysts are shown in Table 3. The concentrations of niobium and nickel were found to be higher on the surface than in the bulk, which is in contrast to the results of the reported Pechini synthesis by Sievers and co-workers.[9] This can be counted as a major advantage of using sol–gel auto-combustion synthesis (SGCS) to synthesize $NiAl_2O_4$-based catalysts, as a high nickel (active sites) exposure on the surface can be achieved. SP-0.06 Nb shows the largest difference between the surface and bulk composition, suggesting that Nb introduction can enhance the nickel exposure on the surface of catalysts to some extent. The $NiNb_2O_6$ phase in these catalysts can also contribute to this observation.

H_2 temperature-programmed reduction (H_2-TPR) data

H_2-TPR analyses were performed to further investigate the effect of Nb doping on the redox properties of the catalysts. The complete reduction of bulk $NiAl_2O_4$ requires a high temperature (> 900 °C) as shown in Figure S1 in the Supporting Information, which is in good agreement with reports.[9,44,45] Deconvolution of the spinel peaks was performed based on the Gaussian model for qualitative investigation purposes.

A small peak at ≈300 °C was observed for all catalysts, which is attributed to the reduction of nickel oxide on the surface of bulk spinel.[9] In addition, the SP catalyst presented a very small peak at 423 °C, which is likely owing to a small quantity of the NiO phase (without any interaction with the spinel surface) that could not be detected by XRD and other characterization techniques used in this study, except XPS.[46] As seen from the deconvolution in Figure S1, two peaks are assigned to the spinel reduction for all catalysts. According to the literature, most of the cubic spinel lattice contains ions in the O_h sub lattice and these have a greater chance of exposure on the surface of these materials.[47] Therefore, it can be postulated that the first reduction peak of spinel ($SP_{[Oh]}$) is related to the available nickel in the O_h sites, and the second corresponds to the nickel ions in T_d sites ($SP_{[Td]}$). The SP and SP-0.10 Nb showed very similar temperatures for $SP_{[Oh]}$ and $SP_{[Td]}$, with a smaller reduction peak seen for $SP_{[Oh]}$ in SP than for SP-0.10 Nb as the only difference. The reduction peak of $SP_{[Oh]}$ became smaller and shifted to a higher temperature in SP-0.02 Nb than for SP, which suggests a lower population of nickel ions in O_h sites for this catalyst. The shift of the $SP_{[Oh]}$ peak in SP-0.06 Nb to higher temperature followed the same trend as seen for SP-0.02 Nb and resulted in the same peak positions of $SP_{[Oh]}$ and $SP_{[Td]}$ for this sample.

A study of the facets that are sensitive to substitution in T_d sites in the XRD and UV–DRS analyses suggested the following order for the population of nickel in the O_h environment: SP ≈ SP-0.10 Nb > SP-0.02 Nb > SP-0.06 Nb. However, the XPS data suggested the following order of increase of defect surface for the spinel: SP-0.02 Nb > SP ≈ SP-0.10 Nb > SP-0.06 Nb. Zhang et al. reported that nickel ions in octahedral sites are reduced more easily than those in tetrahedral sites.[7] Considering the high chance of Ni^{2+} exposure in O_h sites and the suggested population of defect sites from the XPS, it can be stated that the defect sites belong to the O_h environment on the surface of the catalysts and the combination of both effects resulted in complex systems for the observed first TPR analyses.

The catalysts were re-oxidised using oxygen as oxidant. It is well established that nickel atoms in the metallic state leave the lattice of spinel.[11] Each type of generated metallic nickel atom will result in a different type of nickel oxide, and a second TPR can be viewed as a good technique to identify these species. As shown in Figure S2, three different types of NiO were identified after the reduction of the catalysts for the second time. The total peak areas for two of the three formed nickel oxides decrease as the concentration of Nb increases in these catalysts. Furthermore, the peak areas of $SP_{[Oh]}$ decrease as the Nb content of these catalysts increases, suggesting that the presence of nickel in the octahedral sites is diminished by the addition of Nb.

Based on the literature, the first reduction peak (≈190 °C) in the second TPR cycle data can be assigned to the reduction of Ni^{3+}.[46] This peak was only observed in SP and SP-0.02 Nb, which suggests that Ni^{3+} species possibly originated from the sites with octahedral coordination. Also, the peaks at ≈230 °C and 350 °C are assigned to the reduction of different crystallite sizes of NiO with no interaction with the support.[46] It is also well accepted that the NiO peak at temperatures below 400 °C originated from octahedral coordination, whereas the higher temperature peak corresponds to tetrahedrally coordinated NiO supported on alumina.[48] Therefore, the observed peak at 550 °C for SP-0.10 Nb is attributed to large particles of nickel

oxide supported on alumina with tetrahedral coordination.[46,48] The oxygen atoms that are in the O_h sub lattice seem to contribute to the redox properties of these materials, as the peak for Ni in O_h sites was shifted to lower temperatures with shrunken areas when the first and second TPR cycles were compared.

Catalytic data on *n*-octane conversion

A carbon-to-oxygen ratio (C/O) of (8:1) was chosen for this study because conditions that tend more towards anaerobic seem to be more suitable for the ODH of medium-chain paraffins.[49] The under study spinel based catalysts showed relatively good conversions under the chosen operating conditions (Figure 7). At 450 °C and 500 °C, the activities of these catalysts

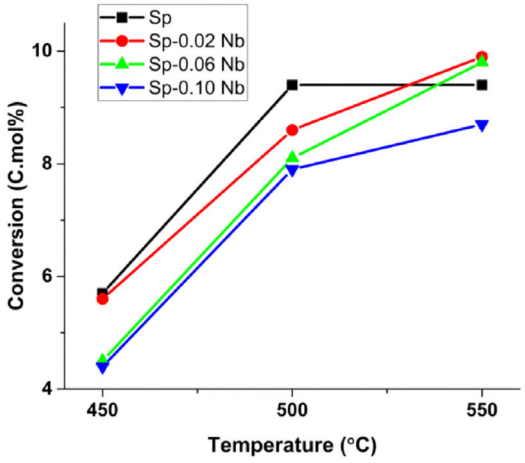

Figure 7. Catalytic conversion of *n*-octane over SP-*x*Nb (*x*: 0, 0.02, 0.06 and 0.10) catalysts. (Reaction conditions: C/O = 8:1, GHSV = 12000 h^{-1}, concentration of *n*-octane in the feed = 11 %).

seem to decrease with an increase in the amount of niobium as a dopant. Indeed, the catalysts containing the highest concentration of Nb atoms showed the lowest activity at 550 °C. $NiNb_2O_6$ seems to be an inert phase (from the redox aspect) in ODH under the chosen reaction conditions. Also, the detected NiO phase in the SP catalyst (based on the first H_2-TPR cycle) in Figure S1, which showed similar catalytic activity as the other catalysts, thus does not appear to contribute to the catalytic process over SP, possibly owing to its fast deactivation caused by hard coke deposition, which will be discussed below with the TGA results.

In addition, the presence of this hard coke likely resulted in the observation of a plateau for conversion over SP if the reaction temperature was increased from 500 to 550 °C.

Selectivity to different products

The selectivity towards octene isomers increased with increasing Nb doping, at all temperatures (Figure 8). However, the selectivity to octene over SP-0.02 Nb was higher than over SP-0.06 Nb. Elevating the reaction temperature seems to have an adverse effect on the selectivity towards octenes, suggesting consecutive cracking and combustion of the primary products to secondary products (aromatics, cracked and CO_x) at high temperatures.

Except for SP-0.06 Nb, the selectivity towards aromatics decreased as the Nb content of these catalysts increased (Figure 8). Also, there is a direct correlation between pore volume and selectivity to aromatics, and SP-0.06 Nb showed the lowest selectivity towards aromatics. Furthermore, the increase of the temperature positively affects the aromatics formation over the two least active catalysts (SP-0.06 Nb and SP-0.10 Nb), whereas the most active catalysts showed a high propensity to crack the formed octenes or aromatics if the temperate was increased to 550 °C from 500 °C.

Olefin cracking is highly dependent on the surface acidity of the catalyst.[24] The catalytic data suggests the lowest selectivity to cracked products was obtained over SP-0.02 Nb, whereas SP showed the highest selectivity to cracked products (Figure 8). This suggests that the substitution of $Ni_{[Oh]}$ sites with Nb resulted in lower selectivity towards cracked products; however, the contributions of $NiNb_2O_6$ to the surface acidity and area, as well as doping, created a complex set of results for interpretation of this catalytic data, which is out of the scope of the current study.

The selectivity towards CO_x seems to exactly follow the order of Nb substitution in the O_h and T_d sites. The two catalysts with similar $Ni_{[Oh]}/Ni_{(Td)}$ ratios, SP and SP-0.10 Nb, showed very similar selectivity to CO_x, whereas the catalyst with low nickel occupation in both sites (SP-0.06 Nb) and low oxygen vacancies as shown by XPS data seems to accelerate the CO_x formation (Figure 8). However, the low concentration of Nb in the O_h lattice of SP-0.02 Nb seems to be beneficial for minimizing selectivity to CO_x and clearly shows an enhanced ODH activity over the catalysts with the highest concentration of defect sites.

The selectivity to aromatic products could provide evidence for the reaction pathways in this system. Ethylbenzene and *o*-xylene are the results of further dehydro-aromatization of different octadienes over the active sites of the catalysts through 1,6 and 2,7 cyclisation.[50] In addition, other isomers of xylene cannot form under the chosen reaction conditions in this study because those require branched octadienes, which form over acidic sites and under a high H_2 pressure.[50] Styrene normally forms from the ODH of ethylbenzene. It seems high temperature (550 °C) is required to form *o*-xylene over all catalysts (Figure 9). Ethylbenzene seems to be the dominant aromatic over SP, whereas catalysts containing Nb seem to give styrene as the dominant aromatic over all temperature ranges (Figure 9). However, a volcano type behaviour was observed in selectivity to ethylbenzene over all catalysts at the different temperatures, suggesting the participation of non-oxidative dehydrogenation (DH) (to form ethylbenzene from octene) over these catalysts, which was in agreement with an increase in the detection of hydrogen (data available in supporting information). The breakdown of selectivity to different octene isomers, CO and CO_2 also can be found in the supporting information. In addition, a comparison of the calculated quantity of

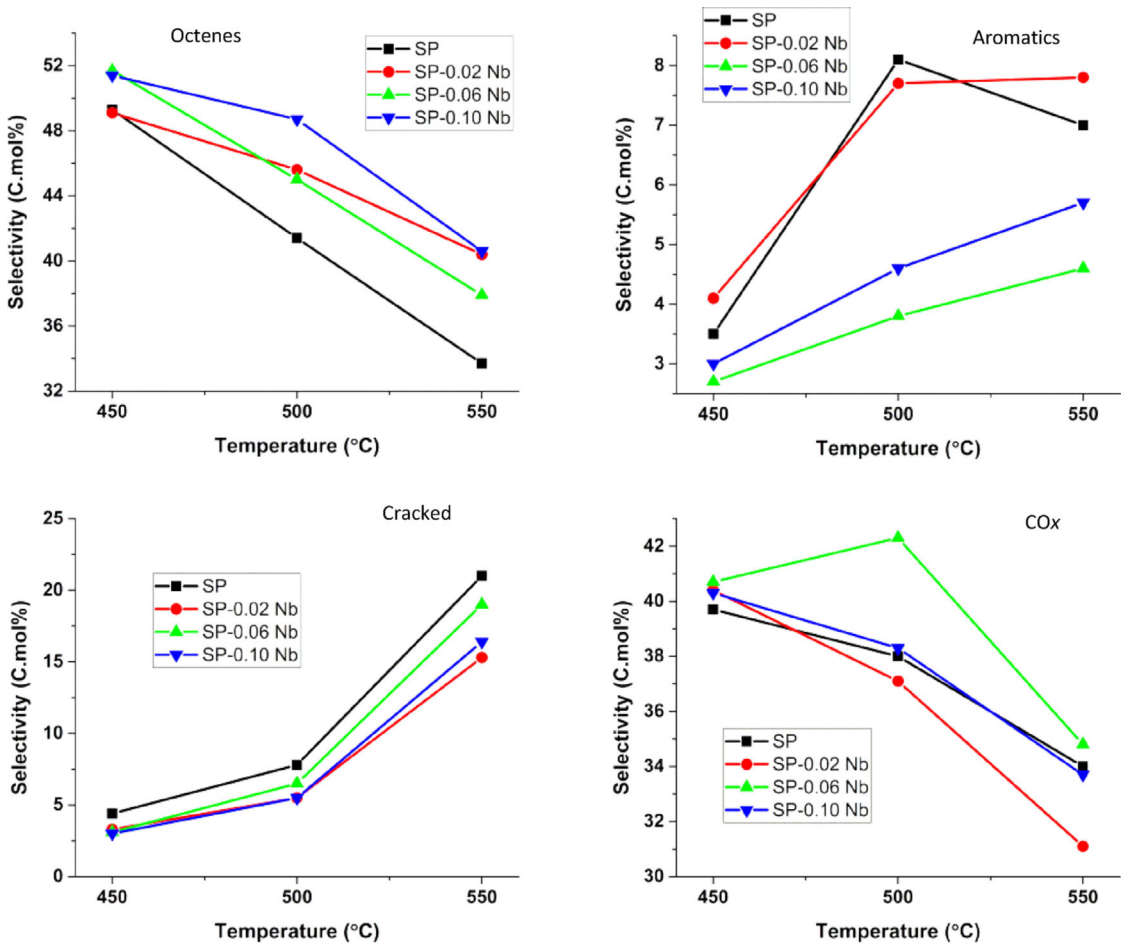

Figure 8. Catalytic selectivity to different products over SP-*x*Nb (*x*: 0, 0.02, 0.06 and 0.10). (Reaction conditions: C/O = 8:1, GHSV = 12 000 h^{-1}, concentration of *n*-octane in the feed = 11 %).

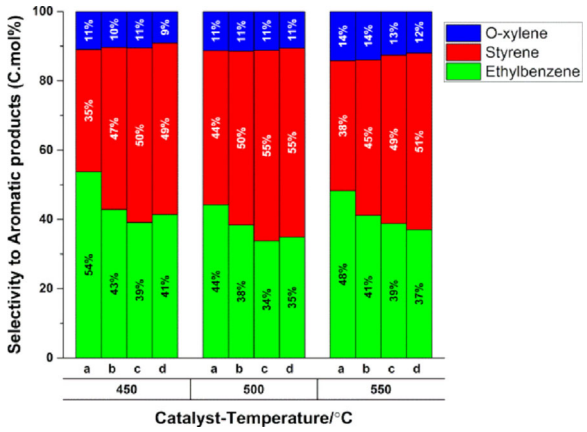

Figure 9. Selectivity towards different aromatic products; a) SP, b) SP-0.02 Nb, c) SP-0.06 Nb and d) SP-0.10 Nb. (Reaction conditions: C/O = 8:1, GHSV = 12 000 h^{-1}, concentration of *n*-octane in the feed = 11 %).

H_2 produced in the product formation and detected H_2 shows (Figure S5) that ODH is dominant over all catalysts and Nb introduction further suppresses the already minor dehydrogenation pathway over SP and promotes the ODH pathway.

TGA analysis of the coked catalysts

Slight coke formation in the unsteady state was expected because the reactions were run under somewhat anaerobic conditions (C/O = 8:1). To determine the catalyst stability and to estimate the possible coking, all catalysts were subjected to a time-on-stream analysis at 500 °C. After reaching steady state (no change in the activity and selectivity observed), the catalysts were run for a further 48 h, showing the stability of these catalysts in time on line applications. The reactor was switched off after 48 h and the catalysts were cooled down under nitrogen and subjected to coke analysis.

The TGA data showed mass losses of 4 %, 2 %, 2 % and 1.5 % for the used SP, SP-0.02 Nb, SP-0.06 Nb and SP-0.10 Nb catalysts, respectively (Figure S6). The data in Figure 10 shows the different types of coke formed on the surface of these catalysts. SP showed two different types of coke that could be removed at 462 °C (soft coke) and 596 °C (hard coke), respectively (Figure 10). However, the small peak attributed to hard coke for this catalyst seems to be for the coke formed on the available NiO phase detected by XPS and H_2-TPR (Figure 6 and Figure S1) in this catalyst because this TGA peak was absent for the other catalysts (Figure 10). This type of coke possibly deactivated the available NiO/Al_2O_3 detected for the SP catalyst be-

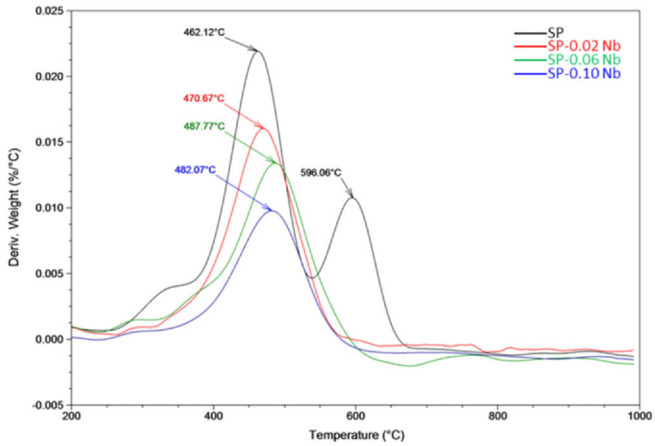

Figure 10. TGA analysis of the used SP-*x*Nb (*x*: 0, 0.02, 0.06 and 0.10) under flow of air. The used catalysts were obtained after 48 h time-on-stream at 500 °C.

cause its combustion temperature is well above the operating temperature (500 °C) for the coking study. The peak corresponding to the soft coke moved slightly to higher temperature with a decrease in peak area upon introduction of Nb in the catalysts. This soft coke is common for all four catalysts, whereas the quantity is different depending on the amount of loaded Nb. This suggests that the caused physicochemical changes in the used catalysts are caused by coking and not vice versa. The observation of mainly soft coke over the used catalysts suggests that in situ coke removal took place under the steady-state conditions, which prevents the formation of hard coke. In addition, other characterisation data of the used catalysts showed a decrease in the crystallite sizes, increase in surface areas and nickel migration between the two sub-lattices of the cubic spinel catalysts during the catalytic testing. Further characterisation was performed to discover the main factors causing these changes during the catalytic applications.

In situ XRD analysis

The in situ XRD data for the fresh SP-0.02 Nb under reduction and oxidation conditions from 100–600 °C is available in Figures S7 and S8. This data suggests no nickel migration or crystallite size change owing to a temperature change under reducing or oxidising conditions and, therefore, some other factors probably cause the observed differences between fresh and used catalysts.

XPS of the used catalyst

The XPS data of the used SP-0.02 Nb is shown in Figure 11. The Ni 2p data shows that three different types of nickel are present on the surface of this catalyst. Ni^{3+} and nickel in octahedral sites seem to be present as was seen for the fresh catalyst, but there is a new peak at 853.5 eV that can be assigned to bulk NiO.[46] Also, the detection of this newly formed NiO was confirmed by the detection of new oxygen species on the surface of this catalyst at 529.6 eV, which can be related to the

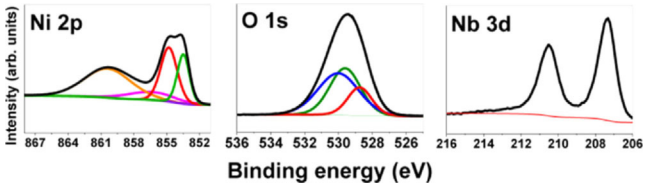

Figure 11. XP spectra of the used SP-0.02 Nb. Deconvolutions of the core-level spectra Ni 2p, O 1s are provided. The used catalysts were obtained after 48 h time-on-stream at 500 °C.

oxygen in NiO (Table 4). The other two oxygen peaks are the same as for the fresh catalyst. Also, no change was observed in the binding energy of the surface niobium in the XPS of the used SP-0.02 Nb catalyst, which proves that this element is not directly involved in the chemistry over the chosen catalytic model reaction.

Table 4. Surface compositions of the used SP-0.02 Nb catalyst determined by XPS. The used catalysts were obtained after 48 h time-on-stream at 500 °C.

	Ni $2p_{3/2}$			O 1s		Nb 3d
Ni^{3+}	$Ni^{2+}{}_{[Oct]}$	NiO	$O_{(ion)}$	O	M–O	(doublet)
856.4	854.8	853.5	530.1	529.6	528.8	210.5–207.4

TEM imaging of the used catalyst

The TEM image of used SP-0.02 Nb was compared to that of the fresh one (Figure 12). This comparison shows the presence of very small crystals (4–5 nm), which are absent in the fresh catalyst. The d spacing in the observed small crystals of the used catalyst (0.2094 nm) is slightly higher than for the fresh catalyst (0.2013 nm), which confirms the presence of NiO[51] of very small size in the used catalysts, as was also evidenced using XPS.

Discussion

Physicochemical and catalytic properties of Nb-doped spinel

Nb has a similar atomic radius to Ni and Al, and was shown to be to partially substituted into the lattice of $NiAl_2O_4$, using the SGCS technique. The Nb increased the crystallite sizes of the $NiAl_2O_4$-based catalysts and decreased their BET surface areas. These simple physical changes seem to affect the catalytic ODH performances and coke deposition over these catalysts. These changes created the opportunity to investigate the effect of coking over this family of catalysts, systematically.

Nb substitution also modified the structure of the $NiAl_2O_4$ spinel. XRD, UV–DRS and XPS data were in excellent agreement to show these structural alterations. Nb prefers to occupy the O_h sub-lattice of spinel if only nickel was replaced by it. Replacing both Ni^{2+} and Al^{3+} with Nb^{5+} resulted in the substitution of this element in both sub-lattices, depending on the existing cationic vacancies in the spinel. Furthermore, and

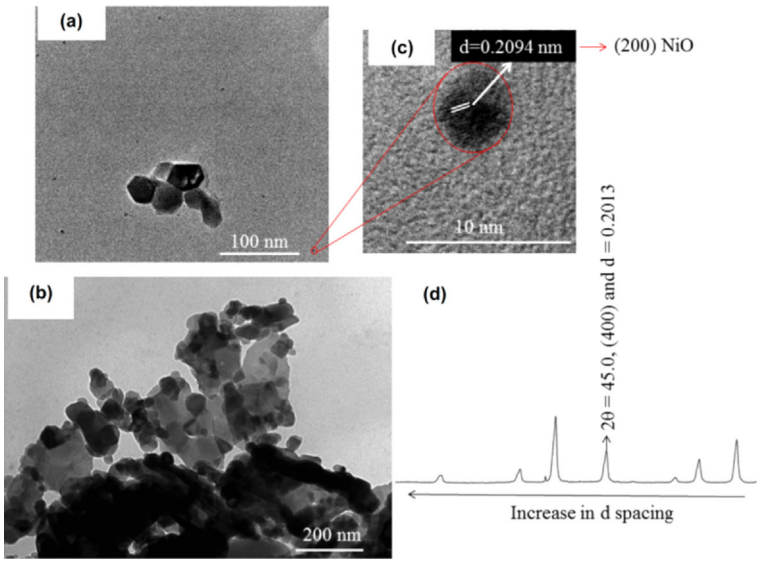

Figure 12. Comparison of the a) used and b) fresh SP-0.02 Nb. c) The lattice fringe (d spacing) of the small crystal (which appeared after the catalytic testing) of the used SP-0.02 Nb was measured using HRTEM and d) compared to the d spacing value obtained from the PXRD pattern for used SP-0.02 Nb. The used catalysts were obtained after 48 h time-on-stream at 500 °C.

based on UV–DRS data, Nb doping in O_h sub-lattices facilitates the migration of nickel from O_h to T_d environments. It has been shown that Nb^{5+} can be a high-valance dopant (HVD) or low-valance dopant (LVD) in the form of $Nb_2O_4^{2-}$ for the outermost lattice of NiO and enhance its ODH catalytic performance in this way.[31] Interestingly, this study showed the high probability of the latter type of dopant existing if a low quantity of Nb was used, because the XPS data showed more ionic oxygen and better catalytic data for this catalyst. The possible low concentration of cationic vacancies, as well as a high degree of $NiNb_2O_6$ formation, seems to result in similar structures for SP and SP-0.10 Nb, because the XRD, UV–DRS and XPS data were similar for them (Scheme S1 in the Supporting Information).

The selectivity to CO_x (undesired product) was found to strongly correlate to the structural profiles of these catalysts. XPS and TPR data showed that the defect sites on the O_h, and these defect sites are believed to be on the outermost surface of spinel, were highest for SP-0.02 Nb. SP-0.02 Nb showed the lowest selectivity to CO_x, whereas SP and SP-0.10 Nb showed similar selectivity to CO_x. Interestingly, SP-0.06 Nb showed the highest selectivity to CO_x and no defect sites were found for this catalyst using XPS. In addition, the H_2-TPR data showed easier reduction of nickel in O_h than T_d sites of spinel, because nickel in O_h sites was mainly reduced if the second TPR was performed for these catalysts.

Effect of coking on Nb-doped $NiAl_2O_4$ spinel

Coking was found to influence both physical and chemical properties of these materials. According to the TGA data, coking of $NiAl_2O_4$ was found to decrease with the increase of Nb content of these catalysts. The TPR studies showed that the reduction of nickel in $NiAl_2O_4$ is only possible at high temperatures (>800 °C), whereas the coke analysis study was done on the catalyst after reaction at 500 °C. The detection of NiO using HRTEM and XPS in the used catalyst indicates that the coking was found to reduce the NiO_x in the lattice of $NiAl_2O_3$ at lower temperatures. Coking also resulted in the reduction of crystallite sizes of these catalysts and improve their surface areas. In addition, coke formation added small shoulders to each peak in the XRD, which implies the formation of $NiAl_2O_4$ with altered characteristics, likely small crystals of $NiAl_2O_4$ with a different lattice strain. The used catalysts also have more Ni in T_d sites than in O_h sites, which is an indication of nickel migration or removal from O_h environments during the catalytic reaction. The lattice fringes of the small observed crystals in the used SP-0.02 Nb proved the formation of small crystals of NiO during the catalytic reactions.

The in situ XRD data showed that thermal changes under reducing or oxidising conditions do not cause these changes. In addition, the XPS data and HRTEM imaging indicated the presence of the NiO phase in the used SP-0.02 Nb catalyst, which could not be detected using XRD analysis. Therefore, the structural changes of $NiAl_2O_4$ during the ODH of *n*-octane under relatively anaerobic conditions are as follows:

1. Coke formation over fresh $NiAl_2O_4$ catalysts with large crystallite size (XRD, HRTEM).
2. Formation of small Nb-doped $NiAl_2O_4$ crystals owing to coke deposition with different lattice strain.
3. Reduction of available vicinal nickel of the defect sites of the O_h sub lattice on the surfaces of large, as well as newly formed small crystals of Nb-doped spinel at low temperature (500 °C) owing to coking.
4. Slow transformation of inverse to normal $NiAl_2O_4$ spinel and formation of NiO under the ODH reaction conditions, upon the consumption of nickel in O_h sites to form NiO and defects.

Conclusions

Niobium seems to preferentially replace the nickel in the octahedral sub-lattice of the spinel. This dopant also was able to replace both Al^{3+} and Ni^{2+}, possibly because of their similar ionic radii. This occupancy resulted in modification of nickel migration, electronic profile, redox properties and surface textures. The crystallite sizes and degree of inversion of the spinel were reduced if the used catalysts were compared to the as-prepared catalysts, indicating that Ni^{2+} in O_h sites is responsible for the observed oxidative dehydrogenation (ODH) performance. The defect sites in the octahedral environment of these catalysts were found to have a positive influence in re-

ducing CO_x formation during ODH of *n*-octane. The slight coke deposition resulted in the appearance of in situ formed $NiAl_2O_4$ with different lattice strain than the fresh catalysts and possible migration of nickel from octahedral to tetrahedral sites of the spinel structure. Coke deposition was also found to facilitate the reduction of nickel in octahedral sites and its slow release into the catalytic system as NiO under the ODH conditions, which may result in the formation of highly defective O_h sites for these spinel-based catalysts.

This study shows the high potential of the binary spinel-based materials with tuneable physicochemical properties and dynamic nature (depending on the reaction conditions), which can be used as a strong tool in heterogeneous catalysis and other applications.

Experimental Section

Materials

The metal precursors used in the synthesis, $Ni(NO_3)_2{\cdot}6H_2O$ (ACS reagent grade), $Al(NO_3)_3{\cdot}9H_2O$ (ACS reagent grade) and $C_4H_4NNbO_9{\cdot}xH_2O$ (99.99% trace metals basis), were used as received from Sigma–Aldrich. Oxalyldihydrazine was freshly synthesised using a reported method.[52] De-ionized water was used throughout the synthesis. *n*-Octane (>98%) was purchased from Alfa Aesar. Synthetic air (UHP) and nitrogen (UHP) were supplied from zero air and N_2 generators (Peak Scientific), respectively, for catalytic testing. Hydrogen (base line), Argon (base line) and Helium (base line) were purchased from Afrox for GC analyses in this study. 10% H_2/Ar and 10% O_2/Ar (Afrox) were used in the TPR–TPO–TPR analysis.

Sol–gel auto combustion synthesis (SGCS) of nickel aluminate catalysts

The stoichiometric amounts of each precursor (including fuel) were weighed and mixed in water. The solution was stirred at 80 °C on a heater stirrer until all starting materials were fully dissolved. The mixture was then dehydrated, which resulted in the formation of a thick gel. The formed gel was put in a muffle furnace (set at 400 °C) under static air for 30 min for ignition, followed by a temperature ramp to 500 °C and this temperature was held for one extra hour. The resultant material was crushed and calcined at 1000 °C under a flow of air for 4.5 h. To insure good homogemicity of the catalyst and to prevent the formation of NiO, the sample was crushed every 1.5 h with a mortal and pestel for 10 min during the calcination at 1000 °C (the total of 4.5 h includes the crushing time). The final colour of the catalyst was sky blue.

As the aim of this study was the synthesis of $NiAl_2O_4$ spinel with Nb as a dopant, the atomic ratio between Al and Ni was kept at approximately 2:1. Nb substitution (of Al or Ni) was calculated based on the charge balance and the final molecular formula of the spinel (AB_2O_4). Therefore, the four catalysts for this study are $NiAl_2O_{4\pm\delta}$, $Ni_{0.98}Al_2Nb_{0.02}O_{4\pm\delta}$, $Ni_{0.97}Al_{1.97}Nb_{0.06}O_{4\pm\delta}$ and $Ni_{0.95}Al_{1.95}Nb_{0.1}O_{4\pm\delta}$, labelled as SP, SP-0.02 Nb, SP-0.06 Nb and SP-0.10 Nb throughout this study.

Oxidative dehydrogenation of *n*-octane

A continuous-flow fixed-bed reactor (in vertical flow mode) was used for catalytic testing. The catalyst particles were loaded in the middle of the isothermal zone in a stainless-steel tube (10 mm ID and 200 mm length). The voids were filled using carborundum (40 gritt, Polychem) to minimize the contribution of homogeneous gas phase reactions.[33] Fresh catalyst, 0.5 mL (≈0.45 g) with a particle size of 300–600 μm diluted with the same volume of carborundum (to eliminate mass-transfer limitations), was used for each set of data. All reactions were performed in the range of 450–550 °C at 50 °C intervals. The molar ratio of carbon to oxygen (C/O) was set at 8:1 with a gas hourly space velocity (GHSV) of 12000 h^{-1}. Air was used as a source of oxygen, nitrogen as the inert "make-up" gas. The flow rates of *n*-octane, air and nitrogen were adjusted to set the GHSV. The concentration of *n*-octane in the reactant steam was 11%. The flow rate of nitrogen and air were controlled using two separate mass flow controllers (Bronkhorst) and *n*-octane was pumped (series II HPLC pump) into a heated reactor line (140 °C) to ensure that *n*-octane is in the gas phase.

All products were analysed offline by gas chromatography (GC). H_2, CO and CO_2 were analysed using a PerkinElmer Clarus 400 GC equipped with a TCD detector and PLOT 1010 column with argon as a carrier gas. Unreacted oxygen was quantified using a PerkinElmer Clarus 500 GC equipped with a TCD and PLOT 5A with helium as a carrier gas. The light products in the gas phase were analysed using a Shimadzu 2121 GC with FID detector and PONA capillary column. H_2 and N_2 were used as carrier gas in this GC. The collected liquid products in the catch-pot were analysed by the aforementioned Shimadzu GC. All reported reactions have 100±1% carbon balances and all reported results are the average of at least two runs under steady state conditions.

Physicochemical characterization

Fresh catalysts were characterized as they were synthesised without any special pre-treatment. Powder X-Ray diffraction (Bruker D8 Advance) with a copper radiation source ($\lambda = 1.5406$ nm) was used to analyse the phase composition of the synthesised materials. X-ray photoelectron spectroscopy measurements were performed on a Thermo Kα XPS equipped with a monochromatic small-spot X-ray source using an aluminum anode $Al_{K\alpha}$ ($h\nu = 1486.6$ eV). The background pressure was 4.9×10^{-8} bar, and 4×10^{-7} bar argon was used during measurement to prevent sample charging. Binding energies were referenced to the sample stage, which contains built in calibration standards of copper, silver, and gold. The bulk composition of the synthesised spinel was confirmed with ICP–OES using a PerkinElmer Precisely Optima 5300DV, after the sample was digested in H_2SO_4 (98%, Merck). BET surface area measurements were done using a Micromeritics Tristar II. Samples were degassed under a flow of N_2 at 200 °C with a Micromeritics flow prep 060 overnight prior to each BET analysis. UV-DRS spectra were collected using a PerkinElmer (Lambda 35, UV/VIS Spectrometer) that was equipped with a Labsphere reflectance spectroscopy accessory. Thermogravimetric analysis was done using a TA instrument (SDT Q600) under a positive flow of air. Temperature-programmed reduction/oxidation/reduction was performed using a Micromeritics 2920 Autochem II analyser using methods reported elsewhere.[53] Catalyst morphology was viewed using a Zeiss Ultra plus Scanning Electron Microscope (SEM). The bulk structures of the catalysts were viewed using a Jeol JEM-1010 Transmission Electron Microscope. A Jeol JEM-2100 High Resolution-Transmission Electron Microscope (HR-TEM) was used in dark field-scanning transmission electron micro-

scope (DFSTEM) mode for elemental distribution analysis (mapping). The used catalysts, after the ODH of *n*-octane reaction at 500 °C after 48 h of time-on-stream, were cooled under nitrogen and then characterised.

Acknowledgements

We thank SASOL and the National Research Foundation, South Africa (NRF) for their financial supports. We also thank the Electron Microscopy Unit at the University of KwaZulu-Natal (Westville campus). Furthermore, M. D. Farahani thanks UKZN for a PhD bursary.

Conflict of interest

The authors declare no conflict of interest.

Keywords: carbon · doping · niobium · oxidation · spinel phases

[1] R. Collongues, D. Gourier, A. Kahn-Harari, A. M. Lejus, J. Thery, D. Vivien, *Annu. Rev. Mater. Sci.* **1990**, *20*, 51 – 82.
[2] W. Chu, W. Yang, L. Lin, *Appl. Catal. A* **2002**, *235*, 39 – 45.
[3] T. H. Gardner, J. J. Spivey, E. L. Kugler, A. Campos, J. C. Hissam, A. D. Roy, *J. Phys. Chem. C* **2010**, *114*, 7888 – 7894.
[4] B. Dou, B. Jiang, Y. Song, C. Zhang, C. Wang, H. Chen, B. Du, Y. Xu, *Fuel* **2016**, *166*, 340 – 346.
[5] N. Salhi, C. Petit, A. Kiennemann, *Stud. Surf. Sci. Catal.* **2008**, *174*, 1335 – 1338.
[6] Y. S. Han, J. B. Li, X. S. Ning, B. Chi, *J. Am. Ceram. Soc.* **2004**, *87*, 1347 – 1349.
[7] K. Zhang, G. Zhou, J. Li, T. Cheng, *Catal. Commun.* **2009**, *10*, 1816 – 1820.
[8] M. Machida, K. Eguchi, H. Arai, *J. Catal.* **1989**, *120*, 377 – 386.
[9] J. L. Rogers, M. C. Mangarella, A. D. D'Amico, J. R. Gallagher, M. R. Dutzer, E. Stavitski, J. T. Miller, C. Sievers, *ACS Catal.* **2016**, *6*, 5873 – 5886.
[10] J. Deng, M. Cai, W. Sun, X. Liao, W. Chu, X. S. Zhao, *ChemSusChem* **2013**, *6*, 2061 – 2065.
[11] N. F. P. Ribeiro, R. C. R. Neto, S. F. Moya, M. M. V. M. Souza, M. Schmal, *Int. J. Hydrogen Energy* **2010**, *35*, 11725 – 11732.
[12] M. D. Farahani, J. Valand, A. S. Mahomed, H. B. Friedrich, *Catal. Lett.* **2016**, *146*, 2441 – 2449.
[13] Y. Kathiraser, W. Thitsartarn, K. Sutthiumporn, S. Kawi, *J. Phys. Chem. C* **2013**, *117*, 8120 – 8130.
[14] I. E. Achouri, N. Abatzoglou, C. Fauteux-Lefebvre, N. Braidy, *Catal. Today* **2013**, *207*, 13 – 20.
[15] C. Fauteux-Lefebvre, N. Abatzoglou, N. Braidy, I. E. Achouri, *J. Power Sources* **2011**, *196*, 7673 – 7680.
[16] D. Li, M. Koike, L. Wang, Y. Nakagawa, Y. Xu, K. Tomishige, *ChemSusChem* **2014**, *7*, 510 – 522.
[17] T. H. Gardner, D. Shekhawat, D. A. Berry, M. W. Smith, M. Salazar, E. L. Kugler, *Appl. Catal. A* **2007**, *323*, 1 – 8.
[18] Z. Boukha, C. Jiménez-González, B. de Rivas, J. R. González-Velasco, J. I. Gutiérrez-Ortiz, R. López-Fonseca, *Appl. Catal. B* **2014**, *158 – 159*, 190 – 201.
[19] H. S. C. O'Neill, W. A. Dollase, C. R. Ross, *Phys. Chem. Miner.* **1991**, *18*, 302 – 319.
[20] C. O. Arean, M. L. R. Martinez, A. M. Arjona, *Mater. Chem. Phys.* **1983**, *8*, 443 – 450.
[21] E. C. O'Quinn, J. Shamblin, B. Perlov, R. C. Ewing, J. Neuefeind, M. Feygenson, I. Gussev, M. Lang, *J. Am. Chem. Soc.* **2017**, *139*, 10395 – 10402.
[22] E. W. McFarland, H. Metiu, *Chem. Rev.* **2013**, *113*, 4391 – 4427.
[23] C. O. Augustin, K. Hema, L. J. Berchmans, R. K. Selvan, R. Saraswathi, *Phys. Status Solidi A* **2005**, *202*, 1017 – 1024.
[24] J. J. H. B. Sattler, J. Ruiz-Martinez, E. Santillan-Jimenez, B. M. Weckhuysen, *Chem. Rev.* **2014**, *114*, 10613 – 10653.
[25] D. Teschner, E. Vass, M. Hävecker, S. Zafeiratos, P. Schnörch, H. Sauer, A. Knop-Gericke, R. Schlögl, M. Chamam, A. Wootsch, A. S. Canning, J. J. Gamman, S. D. Jackson, J. McGregor, L. F. Gladden, *J. Catal.* **2006**, *242*, 26 – 37.
[26] J. McGregor, Z. Huang, E. P. J. Parrott, J. A. Zeitler, K. L. Nguyen, J. M. Rawson, A. Carley, T. W. Hansen, J.-P. Tessonnier, D. S. Su, D. Teschner, E. M. Vass, A. Knop-Gericke, R. Schlögl, L. F. Gladden, *J. Catal.* **2010**, *269*, 329 – 339.
[27] S. G. Sanz, L. McMillan, J. McGregor, J. A. Zeitler, N. Al-Yassir, S. Al-Khattaf, L. F. Gladden, *Catal. Sci. Technol.* **2015**, *5*, 3782 – 3797.
[28] C. H. Collett, J. McGregor, *Catal. Sci. Technol.* **2016**, *6*, 363 – 378.
[29] E. Heracleous, A. A. Lemonidou, *J. Catal.* **2006**, *237*, 162 – 174.
[30] E. Heracleous, A. A. Lemonidou, *J. Catal.* **2010**, *270*, 67 – 75.
[31] X. Sun, B. Li, H. Metiu, *J. Phys. Chem. C* **2013**, *117*, 23597 – 23608.
[32] I. Popescu, Z. Skoufa, E. Heracleous, A. Lemonidou, I.-C. Marcu, *Phys. Chem. Chem. Phys.* **2015**, *17*, 8138 – 8147.
[33] H. B. Friedrich, A. S. Mahomed, *Appl. Catal. A* **2008**, *347*, 11 – 22.
[34] M. I. Fadlalla, H. B. Friedrich, *Catal. Sci. Technol.* **2014**, *4*, 4378 – 4385.
[35] S. Lei, C. Wang, D. Guo, X. Gao, D. Cheng, J. Zhou, B. Cheng, Y. Xiao, *RSC Adv.* **2014**, *4*, 52740 – 52748.
[36] B. Savova, S. Loridant, D. Filkova, J. M. M. Millet, *Appl. Catal. A* **2010**, *390*, 148 – 157.
[37] B. P. Ladgaonkar, A. S. Vaingankar, *Mater. Chem. Phys.* **1998**, *56*, 280 – 283.
[38] P. Priecel, D. Kubička, L. Čapek, Z. Bastl, P. Ryšánek, *Appl. Catal. A* **2011**, *397*, 127 – 137.
[39] J. F. Marco, J. R. Gancedo, M. Gracia, J. L. Gautier, E. Ríos, F. J. Berry, *J. Solid State Chem.* **2000**, *153*, 74 – 81.
[40] H. Ojagh, D. Creaser, S. Tamm, C. Hu, L. Olsson, *Ind. Eng. Chem. Res.* **2015**, *54*, 11511 – 11524.
[41] J. Li, S. Xiong, Y. Liu, Z. Ju, Y. Qian, *ACS Appl. Mater. Interfaces* **2013**, *5*, 981 – 988.
[42] N. Özer, T. Barreto, T. Büyüklimanli, C. M. Lampert, *Sol. Energy Mater. Sol. Cells* **1995**, *36*, 433 – 443.
[43] I. Milošev, T. Kosec, H. H. Strehblow, *Electrochim. Acta* **2008**, *53*, 3547 – 3558.
[44] C. Jiménez-González, Z. Boukha, B. de Rivas, J. R. González-Velasco, J. I. Gutiérrez-Ortiz, R. López-Fonseca, *Energy Fuels* **2014**, *28*, 7109 – 7121.
[45] L. Zhou, Y. Guo, J. M. Basset, H. Kameyama, *Chem. Commun.* **2015**, *51*, 12044 – 12047.
[46] S. R. Kirumakki, B. G. Shpeizer, G. V. Sagar, K. V. R. Chary, A. Clearfield, *J. Catal.* **2006**, *242*, 319 – 331.
[47] J. P. Jacobs, A. Maltha, J. G. H. Reintjes, J. Drimal, V. Ponec, H. H. Brongersma, *J. Catal.* **1994**, *147*, 294 – 300.
[48] C. Li, Y.-W. Chen, *Thermochim. Acta* **1995**, *256*, 457 – 465.
[49] J. Zhang, X. Liu, R. Blume, A. Zhang, R. Schlögl, D. S. Su, *Science* **2008**, *322*, 73 – 77.
[50] E. A. Elkhalifa, H. B. Friedrich, *J. Mol. Catal. A* **2014**, *392*, 22 – 30.
[51] Y. Dong, Y. Chen, P. Jiang, G. Wang, X. Wu, R. Wu, *RSC Adv.* **2016**, *6*, 7465 – 7473.
[52] A. Koch, A. Phukan, O. B. Chanu, A. Kumar, R. A. Lal, *J. Mol. Struct.* **2014**, *1060*, 119 – 130.
[53] V. D. B. C. Dasireddy, H. B. Friedrich, S. Singh, *Appl. Catal. A* **2013**, *467*, 142 – 153.

Manuscript received: December 5, 2017
Revised manuscript received: January 18, 2018
Version of record online: ■■ ■■, 0000

*M. D. Farahani, V. D. B. C. Dasireddy, H. B. Friedrich**

■■ – ■■

Oxidative Dehydrogenation of *n*-Octane over Niobium-Doped $NiAl_2O_4$: An Example of Beneficial Coking in Catalysis over Spinel

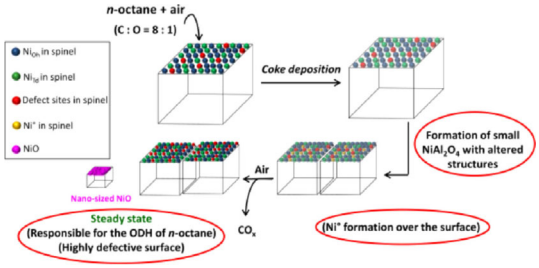

Nickel wanders with coke: Nb-doped $NiAl_2O_4$ catalysts are synthesized and used in the oxidative dehydrogenation (ODH) reaction of *n*-octane. Nickel migration and varying concentration of defect sites are established upon the substitution of Nb and coke deposition.